Hypervirulent Group A Streptococcus of Genotype emm3 Invades the Vascular System in Pulmonary Infection of Mice

Author: Benfang Lei, Dylan Minor, Wenchao Feng, and Mengyao Lui

Lei, Benfang, Dylan Minor, Wenchao Feng, and Mengyao Liu. "Hypervirulent Group A Streptococcus of Genotype emm3 Invades the Vascular System in Pulmonary Infection of Mice." Infection & Immunity 86 (April 2018): e00080-18. DOI:10.1128/IAI.00080-18.

Hypervirulent Group A *Streptococcus* of Genotype *emm*3 Invades the Vascular System in Pulmonary Infection of Mice

Benfang Lei,[a] Dylan Minor,[a] Wenchao Feng,[a] Mengyao Liu[a]

[a]Department of Microbiology and Immunology, Montana State University, Bozeman, Montana, USA

ABSTRACT Natural mutations of the two-component regulatory system CovRS are frequently associated with invasive group A *Streptococcus* (GAS) isolates and lead to the enhancement of virulence gene expression, innate immune evasion, systemic dissemination, and virulence. How CovRS mutations enhance systemic dissemination is not well understood. A hypervirulent GAS isolate of the *emm*3 genotype, MGAS315, was characterized using a mouse model of pulmonary infection to understand systemic dissemination. This strain has a G1370T mutation in the sensor kinase *covS* gene of CovRS. Intratracheal inoculation of MGAS315 led to the lung infection that displayed extensive Gram staining at the alveolar ducts, alveoli, and peribronchovascular and perivascular interstitium. The correction of the *covS* mutation did not alter the infection at the alveolar ducts and alveoli but prevented GAS invasion of the peribronchovascular and perivascular interstitium. Furthermore, the *covS* mutation allowed MGAS315 to disrupt and degrade the smooth muscle and endothelial layers of the blood vessels, directly contributing to systemic dissemination. It is concluded that hypervirulent *emm*3 GAS *covS* mutants can invade the perivascular interstitium and directly attack the vascular system for systemic dissemination.

KEYWORDS CovRS, group A *Streptococcus*, peribronchovascular invasion, hypervirulence, systemic dissemination

The major human pathogen group A *Streptococcus* (GAS) causes diverse infections ranging from common pharyngitis to potentially lethal invasive infections (1). Even though invasive GAS infection is rare, it is a substantial health burden in the United States. It is estimated that 10,649 to 13,434 cases and 1,136 to 1,607 deaths due to invasive GAS infections occur annually in the United States, including bacteremic skin and soft tissue infections, pneumonia, and necrotizing fasciitis and bacteremia without focus (2). Invasive infections often lead to septic shock and streptococcal toxic shock syndrome and are difficult to treat. Contemporary severe invasive infections in the United States are most frequently associated with GAS of the *emm* genotypes *emm*1, *emm*12, *emm*28, *emm*89, and *emm*3 (2). Invasive *emm*3 GAS causes a higher mortality rate than invasive strains of other serotypes (3). Poor understanding of GAS pathogenesis in invasive infections hinders the development of efficacious therapies to treat severe invasive infections. In particular, there is a significant knowledge gap on how invasive GAS disseminates systemically.

Invasive GAS isolates are frequently associated with mutations in the two-component regulatory system of virulence CovRS (4, 5). CovRS negatively regulates many virulence factors (6–8). Natural mutations of the sensor kinase *covS* enhance virulence gene expression, resulting in enhanced innate immune evasion, systemic dissemination, and hypervirulence (9–16). How CovRS mutations enhance systemic dissemination is not well understood. Here we report that MGAS315, a hypervirulent *emm*3 GAS strain carrying a G457V missense mutation of the CovS (14), can invade the vascular system

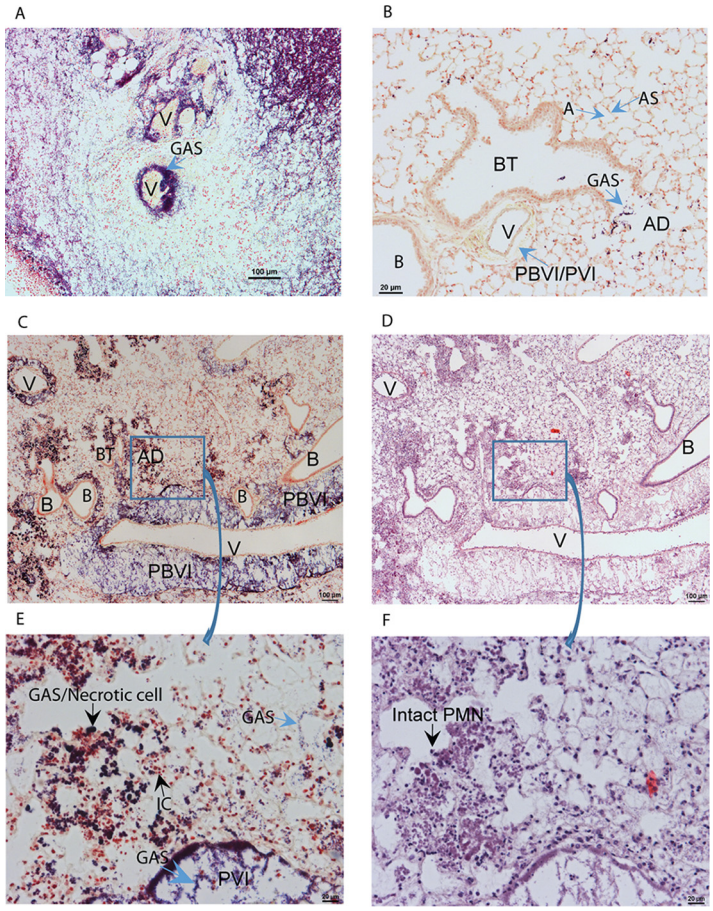

FIG 1 MGAS315 invades the peribronchovascular and perivascular interstitium in pulmonary infections. MGAS315 (10^8 CFU) was inoculated into mice subcutaneously (IS) or intratracheally (IT), and the skin infection site in IS and the lung in IT were collected at 24 h and at 30 min or 32 h, respectively, after inoculation. Thin sections of the samples were stained with Gram or H&E stains. (A to C) Gram stain images for the skin site in IS infection (A) and the lung at 30 min (B) and 32 h (C) after IT inoculation. (D) H&E stain image for the 32-h lung sample. The boxed areas in panels C and D are shown at a magnification of ×20 in panels E and F, respectively. Bacteria and inflammatory cells were stained in blue or dark blue and pink, respectively, in Gram stain. Abbreviations: A, alveoli; AS, alveolar septa; AD, alveolar duct; B, bronchiole; BT, bronchial terminus; PBVI, peribronchovascular interstitium; PVI, perivascular interstitium; V, blood vessel.

in a mouse model of pulmonary infection and that the CovS mutation is required for vascular invasion and enhances systemic dissemination.

RESULTS

MGAS315 invasion of the peribronchovascular and perivascular interstitium. GAS bacteria were found to be enriched around the blood vessels at skin inoculation sites in subcutaneous MGAS315 infection (Fig. 1A). It is possible that MGAS315 can invade the vascular system. This possibility could not be conveniently examined in the mouse model of subcutaneous infection because GAS was inoculated at high density at a focal point. Intratracheal inoculation of MGAS315 was thus used to examine the capacity of MGAS315 to invade the vascular system on the rationale that bacteria would be distributed throughout the lung at low densities after they were breathed in. The mouse lung has 5 lobes. As shown in Fig. 1B and C, thin sections of the lobes in histological analyses typically have bronchioles, bronchial termini that are followed by alveolar dust, alveoli that are separated by alveolar septa, artery and vein vessels, and peribronchovascular and perivascular interstitium. The peribronchovascular interstitium is the connective-tissue sheath that encloses the bronchi, pulmonary arteries, veins, and lymphatic vessels, whereas the perivascular interstitium extended from the

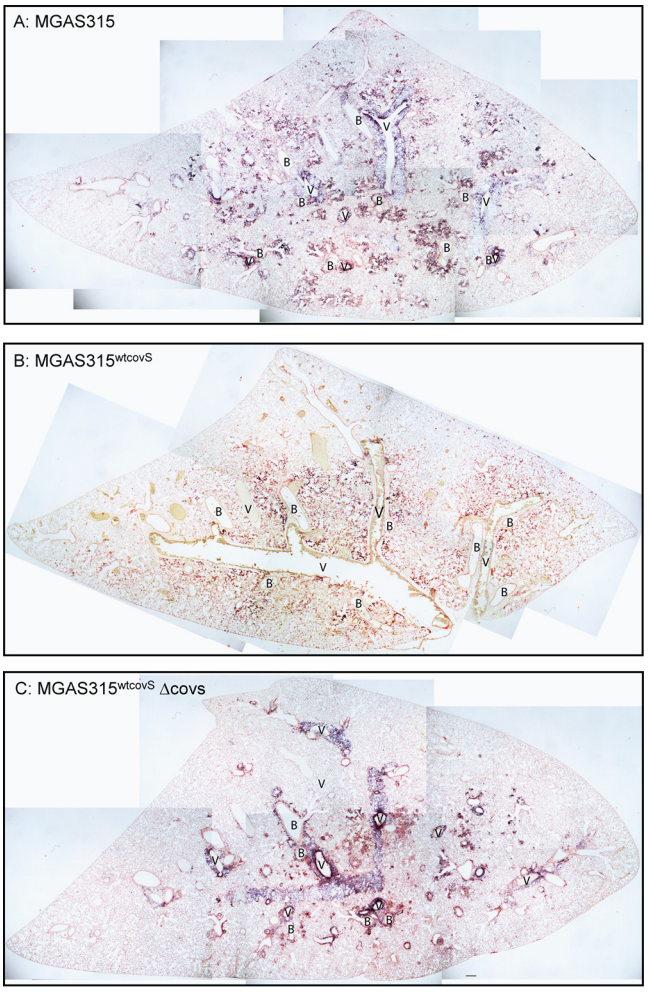

FIG 2 Gram stain images of a whole section of a lung lobe from moribund mice with intratracheal inoculation of 10^8 CFU MGAS315 (A), MGAS315^{wtcovS} (B), and MGAS315^{wtcovS} Δ*covS* (C). The mice became moribund and were euthanized at between 30 and 48 h after inoculation. Each lobe was positive in Gram staining. Shown is a representative Gram stain image of an entire section of a lobe that was generated by compiling multiple partially overlapped image shots along particular tissue marks. Abbreviations: B, bronchiole; V, blood vessel.

peribronchovascular interstitium protects blood vessels that connect the microvasculature system in the alveolar region with the arteries and veins inside the peribronchovascular interstitium. At 30 min after MGAS315 inoculation, GAS bacteria were sparsely scattered along the alveolar ducts and alveolar septa (small blue spots in Fig. 1B). At 24 to 48 h after inoculation, infected mice were all moribund, and each lobe of the lung in each mouse had intense Gram staining for GAS. A representative image of a whole section of one lobe is shown in Fig. 2A. Alveolar ducts were often severely damaged and contained large numbers of bacteria, bacteria were associated with the septa of alveoli, and, more strikingly, intensive Gram staining for GAS was present in the peribronchovascular and perivascular interstitium (Fig. 1C and E and 2). Necrotic and intact neutrophil cells were present at alveolar ducts, whereas there were fewer inflammatory cells in alveoli and peribronchovascular interstitium (Fig. 1D and F). Thus, MGAS315 has the capacity to invade the peribronchovascular interstitium.

CovS mutation of MGAS315 is required for the peribronchovascular and perivascular invasion. MGAS315 has a natural *covS* G1370T mutation, which results in a CovS G457V missense mutation (14). This *covS* G1370T mutation contributes to the hypervirulence of MGAS315 in subcutaneous infection of mice (14). An isogenic strain derived from MGAS315 that carries the wild-type *covS* gene (MGAS315^{wtcovS}) was

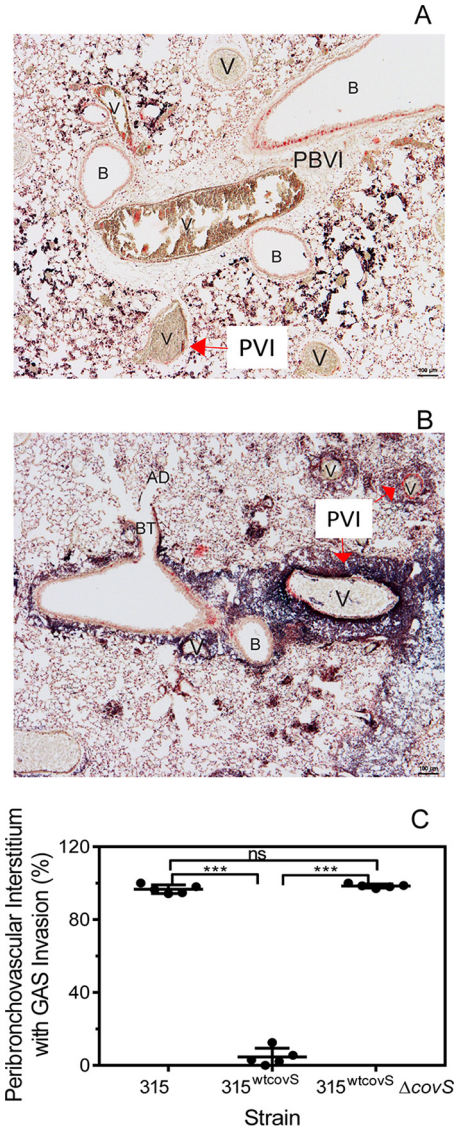

FIG 3 The *covS* G1370T mutation is critical for MGAS315 invasion of the peribronchovascular and perivascular interstitium. (A and B) Representative Gram stain images of thin lung sections from moribund mice after intratracheal MGAS315^{wtcovS} (A) and MGAS315^{wtcovS} Δ*covS* (B) inoculation. Abbreviations: AD, alveolar duct; B, bronchiole; BT, bronchial terminus; PVBI, peribronchovascular interstitium; PVI, perivascular interstitium; V, blood vessel. (C) Percentage of the perivascular interstitium with intensive GAS staining in the lung of moribund mice with IT inoculation of MGAS315, MGAS315^{wtcovS}, and MGAS315^{wtcovS} Δ*covS*. Each dot represents the average value of a mouse in one section of each of all the lobes in GAS-positive regions. Mann Whitney *t* test: ns, not significant; ***, $P < 0.001$.

tested for its ability to cause pulmonary infection and peribronchovascular and perivascular invasion. Like in the MGAS315 infection, mice inoculated intratracheally with 8.6×10^7 CFU of MGAS315^{wtcovS} were moribund by up to 48 h after inoculation. While MGAS315 invaded 96.7% of the perivascular interstitium, MGAS315^{wtcovS} caused infections in alveolar ducts and septa but invaded only 4.6% of the perivascular interstitium (Fig. 2B and 3A and C). Deletion of the *covS* gene in MGAS315^{wtcovS} restored the infection of the peribronchovascular and perivascular interstitium (Fig. 2C and 3B and C). Thus, the inability of MGAS315^{wtcovS} to infect the peribronchovascular and perivascular interstitium was caused by the replacement of the *covS*^{G1370T} mutant gene with the wild-type *covS* gene but not by a spurious mutation that might have been acquired during the construction of MGAS315^{wtcovS}.

The replacement of *covS*^{G1370T} with wild-type *covS* reduced the expression of CovRS-controlled virulence genes (14). Many of the CovRS-controlled virulence factors

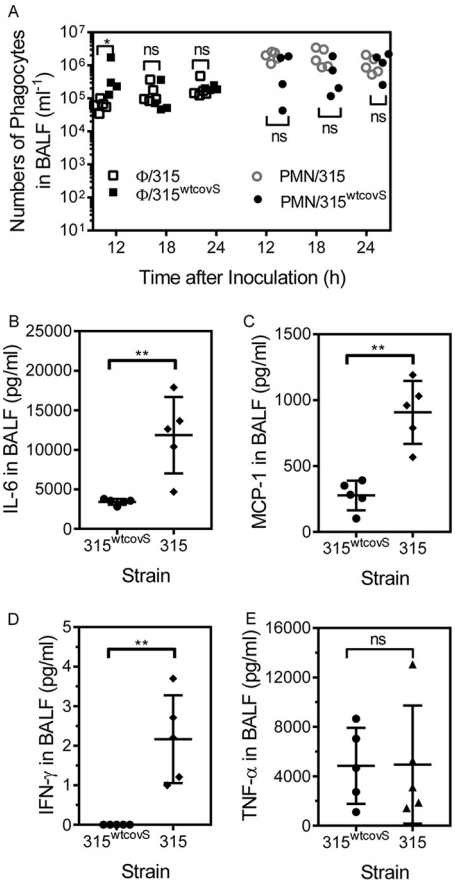

FIG 4 Levels of macrophages, neutrophils, cytokines, and MCP-1 in bronchial alveolar fluid in pulmonary MGAS315 and MGAS315^{wtcovS} infections. (A) BALF samples were collected from mice at the indicated times after intratracheal inoculation of 10^8 CFU of MGAS315 or MGAS315^{wtcovS}. PMN and Φ refer to neutrophils and macrophages, respectively. (B to E) Cytokines and MCP-1 in BALF at 12 h after IT inoculation. MGAS315 versus MGAS315^{wtcovS} Mann Whitney *t* test: ns, not significant; *, $P < 0.05$; **, $P < 0.01$.

are involved in innate immune evasion. So, we compared the numbers of neutrophils, macrophages, and cytokines in bronchoalveolar lavage fluids (BALF) collected at 12, 18, and 24 h after intratracheal inoculation of MGAS315 and MGAS315^{wtcovS}. There were significantly more macrophages in BALF of mice infected with MGAS315^{wtcovS} than with MGAS315 at 12 h but not at 18 h and 24 h after inoculation. There were fewer neutrophils in BALF from MGAS315^{wtcovS} infection than MGAS315 infection at 12 h and 18 h, but the differences were insignificant (Fig. 4A). MGAS315 induced higher levels of interleukin-6 (IL-6), gamma interferon (IFN-γ), and monocyte chemoattractant protein 1 (MCP-1) at 12 h after inoculation than MGAS315^{wtcovS} (Fig. 4). However, histology analyses indicate that the neutrophil responses were not robust in either of the two infections (Fig. 2). These data suggest that innate immune responses might not be the primary reason for the inability of MGAS315^{wtcovS} to invade the perivascular interstitium. To further test this possibility, neutropenic mice were tested. C57BL/6J mice were treated with anti-Ly6G antibody RB6-C85 to deplete neutrophils and inflammatory monocytes (13, 17) or control antibody LTF-2 and then infected with MGAS315^{wtcovS}. The RB6-8C5 treatment reduced neutrophil levels in BALF by 80% (Fig. 5A) but did not enable MGAS315^{wtcovS} to invade the perivascular invasion (Fig. 5C). Thus, the inability of MGAS315^{wtcovS} to invade the perivascular interstitium is not due to neutrophil responses.

Vascular invasion and systemic dissemination. As MGAS315 invades the perivascular interstitium, the integrity of the smooth muscle and endothelial layers lining the

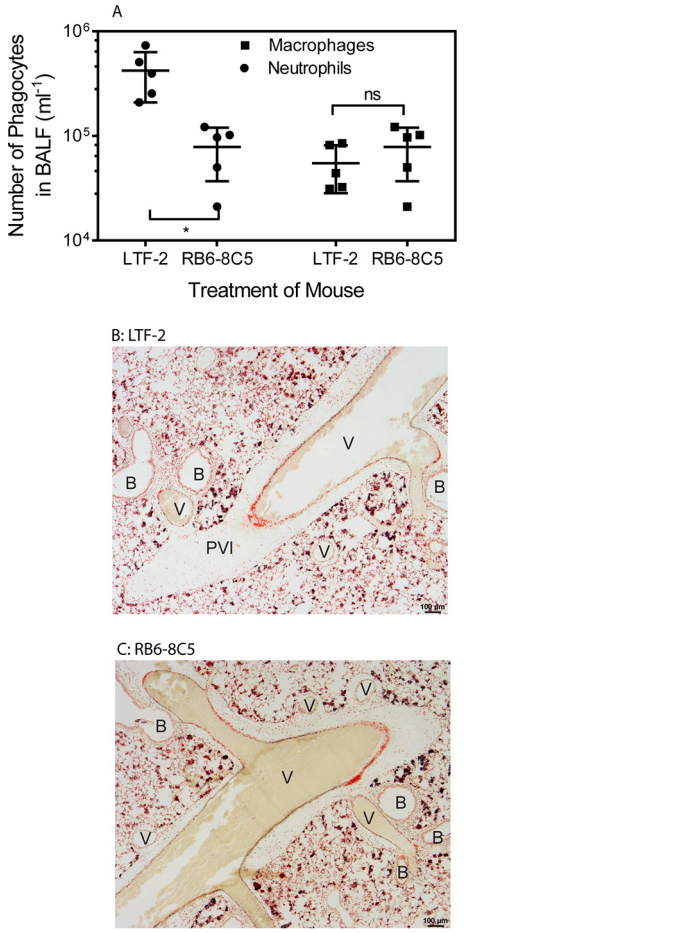

FIG 5 Depletion of neutrophils of C57BL/6J mice does not lead to the invasion of the perivascular interstitium in pulmonary MGAS315^{wtcovS} infection. Mice were injected intraperitoneally with anti-Ly6G MAb RB6-8C5 or isotype control MAb LTF-2 and, 24 h later, were inoculated at the trachea with 10^8 CFU MGAS315^{wtcovS}. (A) Numbers of neutrophils and macrophages in BALF collected at 6 h after GAS inoculation as determined by cytospin analysis. (B and C) Representative Gram stain images of lung sections of mice with MGAS315^{wtcovS} infection after MAb treatment with LTF-2 (control) (B) or RB6-8C5 (C). Abbreviations: B, bronchiole; PVI, perivascular interstitium; V, blood vessel.

blood vessels became disrupted and separated (Fig. 6A). As segments of the smooth muscle and endothelial layers were further degraded, the bacteria were able to enter the lumen of the blood vessels (Fig. 6B). In contrast, blood vessels were intact because MGAS315^{wtcovS} bacteria infected the alveolar region but did not enter the connective-tissue sheath around blood vessels (Fig. 6C), and the depletion of neutrophils and inflammatory monocytes prior to MGAS315^{wtcovS} inoculation did not lead to vascular invasion (Fig. 6D). Deletion of the *covS* gene in MGAS315^{wtcovS} restored the vascular invasion (Fig. 6E). To determine whether MGAS315 invasion of the vascular system plays a critical role in the systemic dissemination of GAS, we compared GAS loads in the lung, liver, and spleen at 24 h after intratracheal inoculation of MGAS315, MGAS315^{wtcovS}, and MGAS315^{wtcovS} Δ*covS*. There was a 4.8-fold-higher MGAS315 load than MGAS315^{wtcovS} load in the lung, whereas there were 6,500- and 1,200-fold higher loads of MGAS315 than of MGAS315^{wtcovS} in the liver and spleen, respectively (Fig. 6F). Apparently, the effects of the *covS* mutation in MGAS315 on GAS loads in the liver and spleen are more profound than on the GAS load in the lung. These data support a critical role of the vascular invasion in systemic MGAS315 dissemination.

MGAS315^{wtcovS} but not MGAS315 forms aggregates with amorphous material along alveolar septa. In MGAS315 infection, bacteria were attached to the alveolar septa (Fig. 7A) and the fibrous matrix in the peribronchovascular and perivascular

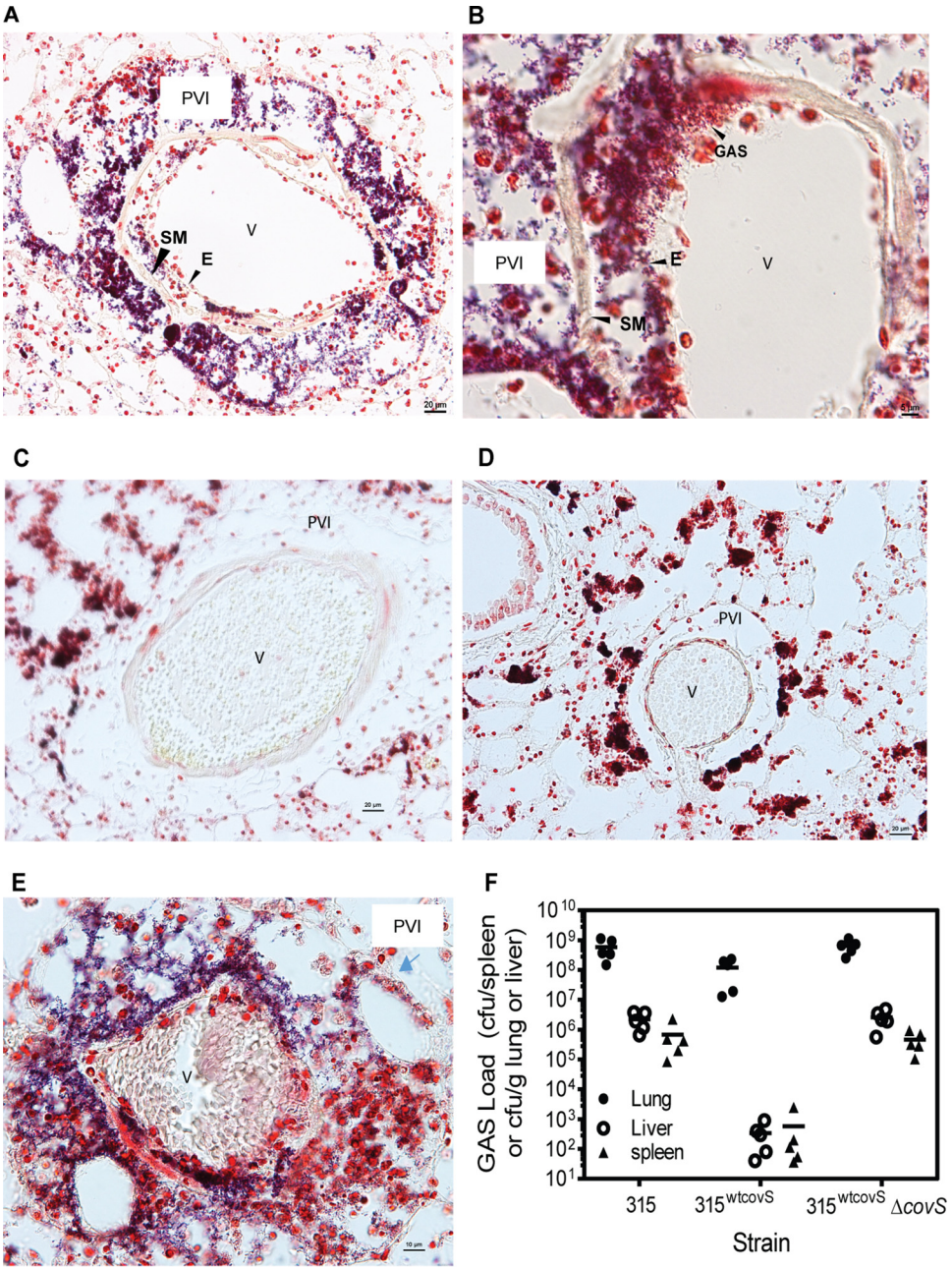

FIG 6 MGAS315 and MGAS315^{wtcovS} Δ*covS* invasion of the perivascular interstitium facilitates the development of damage to the vascular system and systemic GAS dissemination. (A to E) Closeup Gram stain images around some blood vessels in the lung with intratracheal inoculation of MGAS315 (A and B), MGAS315^{wtcovS} (C), and MGAS315^{wtcovS} Δ*covS* (E) in mice and inoculation of MGAS315^{wtcovS} in RB6-8C5-treated mice (D). Abbreviations: E, endothelial cell layer; PVI, perivascular interstitium; SM, smooth muscle; V, blood vessel. (F) GAS loads in the lung, liver, and spleen of mice at 24 h after IT inoculation of 10^8 CFU MGAS315, MGAS315^{wtcovS}, and MGAS315^{wtcovS} Δ*covS*.

interstitium (Fig. 7B) and associated with necrotic cells along the alveolar ducts (Fig. 7C). MGAS315^{wtcovS} Δ*covS* also showed these phenotypes (Fig. 6E). In contrast, in MGAS315^{wtcovS} infection, bacteria formed primarily aggregates that usually were associated with part of the alveolar septa (Fig. 7D). The aggregates contained materials that were stained pink in both Gram and hematoxylin and eosin (H&E) stains but often did not contain nucleus staining (Fig. 7E). Depletion of neutrophils and inflammatory cells with RB6-8C5 treatment of mice did not affect the MGAS315^{wtcovS} aggregation (Fig. 7F). These results suggest that an amorphous material is involved in the formation

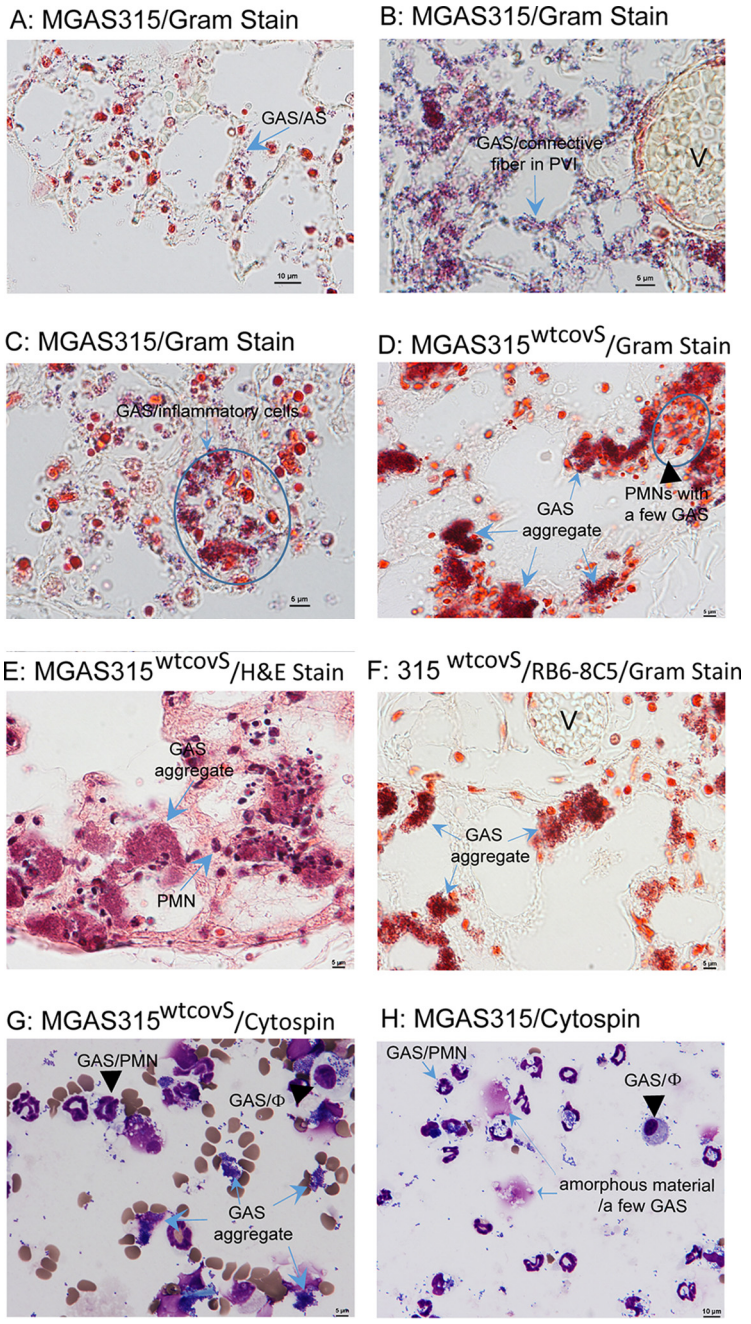

FIG 7 MGAS315^{wtcovS}, but not MGAS315, forms aggregates in alveoli. (A to C) Closeup Gram stain images of the MGAS315-infected lung sample in Fig. 2A showing Gram-positive cocci associated with the alveolar septa (A), fibrous matrix in the perivascular interstitium (B), and inflammatory cells (C). (D to F) Closeup Gram and H&E stain images showing that MGAS315^{wtcovS} forms aggregates with amorphous material in alveoli of mice without and with RB6-8C5 treatment. (G and H) Images of cytospin analyses showing aggregates of MGAS315^{wtcovS} with amorphous material (G) and free and neutrophil-associated MGAS315 bacteria (H) in BALF samples that were collected from mice at 12 h after intratracheal GAS inoculation. PMN and Φ refer to neutrophils and macrophages, respectively.

of the MGAS315^{wtcovS} aggregates. To test this possibility, we performed the cytospin analysis of the BALF samples collected from mice at 12 h after intratracheal MGAS315 and MGAS315^{wtcovS} inoculation. MGAS315^{wtcovS} bacteria in the BALF samples were primarily in aggregates with amorphous materials (Fig. 7G). In contrast, MGAS315 bacteria in the BALF samples were primarily free or associated with neutrophils, and amorphous materials had a few bacteria (Fig. 7H). Thus, MGAS315^{wtcovS}, but not

MGAS315 and MGAS315^{wtcovS} Δ*covS*, forms aggregates with amorphous material in the lung. The identity of this amorphous material is not known.

DISCUSSION

The major finding of this study is that MGAS315 invades the perivascular interstitium and directly attacks the vascular system. The finding is significant in understanding the pathogenesis of invasive *emm*3 GAS. The *emm*3 genotype is one of the most frequent *emm* genotypes that are associated with severe invasive infections (2), and *emm*3 GAS particularly causes more lethal infections (3). Invasive *emm*3 GAS isolates have significantly more CovS mutations than do *emm*3 pharyngitis isolates (5), and CovS mutations are present in more than 50% of invasive *emm*3 GAS isolates in two different clinical strain collections (4, 5). This study demonstrates for the first time that hypervirulent *emm*3 GAS CovS mutants can invade the vascular system. This vascular invasion apparently plays a role for systemic dissemination. Our results illustrate a systemic dissemination mechanism in which hypervirulent *emm*3 GAS CovS mutants directly attack the vascular vessels to access the circulatory system.

Another finding of this study is that the perivascular invasion requires the CovS mutation. CovRS mutations enhance the expression of virulence genes and maximize the potential of GAS to evade neutrophil responses, resulting in GAS mutants with enhanced survival and hypervirulence (9–16). However, the depletion of neutrophils does not lead to the perivascular invasion in MGAS315^{wtcovS} infection. The role of CovS mutations in the perivascular invasion appears not to be directly linked to GAS evasion of neutrophil and inflammatory monocyte responses. MGAS315^{wtcovS}, but not MGAS315, forms aggregates with an amorphous material along the alveolar septa, and the aggregate formation may prevent MGAS315^{wtcovS} from crossing the barrier between the alveoli and the peribronchovascular and perivascular interstitium. Alternatively, MGAS315 may enter the peribronchovascular interstitium by crossing the epithelium in bronchioles. In addition, the damages on the smooth muscle and endothelial layers may involve CovRS-controlled virulence factors. MGAS315 invasion of the vascular system likely involves coordinated actions of multiple virulence factors that are controlled by CovRS. We are currently in the process of elucidating the molecular mechanisms of the perivascular and vascular invasion and prevention of GAS aggregation in alveoli by hypervirulent *emm*3 GAS.

A variety of mouse models of GAS infections have been used to investigate GAS pathogenesis and to evaluate GAS vaccine candidates, including infections through intranasal (18), intraperitoneal (19), air sac (20), intratracheal (21), subcutaneous (22), and intramuscular (23) inoculations. The intratracheal murine pneumonia model used in this study is similar to the intratracheal murine pneumonia model developed by Husmann et al., in which a spontaneous streptomycin-resistant derivative of the M50 GAS strain B514, a natural mouse isolate, induces bronchopneumonia in C3HeB/FeJ mice (21). This B514 derivative, B514-sm, induces robust neutrophil recruitment in the alveoli; Gram-positive cocci in short chains are present within the inflammatory exu-date; and the perivascular interstitium is edematous and contains some neutrophils but not bacteria. These histopathological features of B514-sm-infected lung are different from those in our MGAS315 and MGAS315^{wtcovS} infections of C57BL/6J mice. The intratracheal murine pneumonia model is a valuable model to investigate the patho-genesis of GAS with different genetic backgrounds and the mechanisms of vascular invasion and systemic dissemination. This murine pneumonia model may also be valuable to study the GAS tissue tropism. GAS commonly causes upper but not lower respiratory tract infection. However, 16% of severe invasive GAS infections in the United States are pneumonia (2). Further studies using the pulmonary infection model may elucidate the reason why noninvasive upper respiratory GAS infections usually do not result in lower respiratory infections while certain GAS strains can cause pneumonia.

In conclusion, using an intratracheal murine pneumonia model of GAS infection, we demonstrated for the first time that hypervirulent *emm*3 GAS invades the

peribronchovascular interstitium and attacks the vascular system and that the perivascular and vascular invasion requires CovS mutation and contributes to systemic dissemination.

MATERIALS AND METHODS

Declaration of ethical approval. All animal procedures were carried out in strict accordance with the recommendations in the *Guide for the Care and Use of Laboratory Animals* of the National Institutes of Health (24). The protocol for the experiments was approved by the Institutional Animal Care and Use Committee at Montana State University (permit number 2014-45).

Bacterial strains and growth. Genotype *emm*3 GAS strain MGAS315 with a natural *covS* G1370T mutation and its derivative strain MGAS315^{wtcovS} with the correction of the *covS* mutation have been described previously (14, 25). These strains were grown in 5% CO_2 in Todd-Hewitt broth supplemented with 0.2% yeast extract (THY).

Generation of MGAS315^{wtcovS} Δ*covS*. MGAS315^{wtcovS} Δ*covS* was generated using the suicide plasmid p740-Δ*covS* (14), as described previously (26). The mutant lacked a 1,290-bp internal fragment of the *covS* gene from base 115 to base 1,404 and was confirmed by DNA sequencing.

Pulmonary infection and analyses. GAS bacteria at the exponential growth phase were harvested by centrifugation and washed three times with pyrogen-free Dulbecco's phosphate-buffered saline (DPBS) and resuspended in DPBS at an optical density at 600 nm (OD_{600}) of 3.0. The GAS suspension (100 μl) was then inoculated through a syringe with a blunt-ended needle that was inserted into the trachea of 8-week-old female C57BL/6J mice that were anesthetized through 5% isoflurane inhalation and placed in the supine position on an angled platform with the mouth being gently held open. Actual inocula were determined by plating. When mice became moribund within 48 h after inoculation, they were euthanized with a gradual fill method at a displacement rate of 30% CO_2 of the chamber volume per minute, as recommended in the 2013 American Veterinary Medical Association guidelines. The lung, liver, and spleen were then collected for histological analyses or measurements of GAS loads.

Histological analyses. The lung of euthanized mice was perfused with 10% formalin and fixed in 10% formalin for 24 h, dehydrated with ethanol, cleared with xylene, and infiltrated with paraffin using a tissue embedding console system (Sakura Finetek, Inc.). The paraffin blocks were processed to obtain 4-μm sections, which were stained with H&E or with a Gram stain kit from Becton, Dickinson and Company. Stained slides were examined using a Nikon Eclipse 80i microscope. To obtain the images in Fig. 2, multiple partially overlapped images were taken for a whole lung lobe section, spliced along particular tissue marks, and aligned along the tissue marks to get the compiled image of the entire lung lobe section.

Neutrophil depletion. Rat anti-murine Ly6G monoclonal antibodies (MAb) RB6-8C5 (13, 17) and isotype control MAb LTF-2 were purchased from Bio X Cell. To deplete neutrophils, 250 μg RB6-8C5 in 0.5 ml DPBS was injected into the intraperitoneal cavity of each of the female C57B/6 mice (5 weeks old) at 24 h prior to GAS inoculation. Control mice were treated similarly with LTF-2.

Cytospin analysis. MGAS315 or MGAS315^{wtcovS} (0.1 ml of bacterial suspension in DPBS with an OD_{600} of 3.0) was inoculated in the trachea of female C57BL/6J mice. The mice were euthanized at different times after inoculation, and the lung was lavaged with 1 ml of DPBS to collect BALF. An aliquot of the recovered lavage fluid was used to determine the total number of viable cells by trypan blue exclusion counts. A second aliquot of the recovered lavage fluid at an appropriate dilution was used to prepare cytospin slides using a Shandon Cytospin cytocentrifuge. The slides were stained using the Diff-Quik stain kit from Fisher Scientific. Neutrophils and macrophages among 150 host cells on each cytospin slide were counted to determine the percentage of neutrophils and macrophages, and the total numbers of neutrophils and macrophages were calculated from the percentage data and the total counts of viable cells in the lavage samples.

Cytokine measurements. Groups of five 6-week-old female C57BL/6J mice were inoculated with 0.1 ml of MGAS315 and MGAS315^{wtcovS} at an OD_{600} of 3.0. The mice were euthanized with CO_2 for 12 h after intratracheal inoculation, and BALF was collected. The BALF samples were filtered through 0.2-μm filters and frozen until they were analyzed. Fifty microliters of each sample was used to measure tumor necrosis factor alpha (TNF-α), IFN-γ, IL-6, and MCP-1 using BD cytometric bead array mouse Th1/Th2/Th17 and IL-1β cytokine kits by following the procedures in the manufacturer's manual.

Statistical analyses. The statistical analyses were done using the Mann-Whitney *t* test of the GraphPad Prism software (version 7.03).

ACKNOWLEDGMENTS

This work was supported in part by grants AI095704 and GM110732 from the National Institutes of Health, Montana University System Research Initiative 51040-MUSRI2015-03, and the Montana State Agricultural Experimental Station.

REFERENCES

1. Carapetis JR, Steer AC, Mulholland EK, Weber M. 2005. The global burden of group A streptococcal diseases. Lancet Infect Dis 5:685–694. https://doi.org/10.1016/S1473-3099(05)70267-X.

2. Nelson GE, Pondo T, Toews KA, Farley MM, Lindegren ML, Lynfield R, Aragon D, Zansky SM, Watt JP, Cieslak PR, Angeles K, Harrison LH, Petit S, Beall B, Van Beneden CA. 2016. Epidemiology of invasive group A

streptococcal infections in the United States, 2005-2012. Clin Infect Dis 63:478–486. https://doi.org/10.1093/cid/ciw248.
3. Sharkawy A, Low DE, Saginur R, Gregson D, Schwartz B, Jessamine P, Green K, McGeer A, Ontario Group Streptococcal Study Group A. 2002. Severe group A streptococcal soft-tissue infections in Ontario: 1992–1996. Clin Infect Dis 34:454–460. https://doi.org/10.1086/338466.
4. Ikebe T, Ato M, Matsumura T, Hasegawa H, Sata T, Kobayashi K, Watanabe H. 2010. Highly frequent mutations in negative regulators of multiple virulence genes in group A streptococcal toxic shock syndrome isolates. PLoS Pathog 6:e1000832. https://doi.org/10.1371/journal.ppat.1000832.
5. Shea PR, Beres SB, Flores AR, Ewbank AL, Gonzalez-Lugo JH, Martagon-Rosado AJ, Martinez-Gutierrez JC, Rehman HA, Serrano-Gonzalez M, Fittipaldi N, Ayers SD, Webb P, Willey BM, Low DE, Musser JM. 2011. Distinct signatures of diversifying selection revealed by genome analysis of respiratory tract and invasive bacterial populations. Proc Natl Acad Sci U S A 108:5039–5044. https://doi.org/10.1073/pnas.1016282108.
6. Levin JC, Wessels MR. 1998. Identification of *csrR/csrS*, a genetic locus that regulates hyaluronic acid capsule synthesis in group A *Streptococcus*. Mol Microbiol 30:209–219. https://doi.org/10.1046/j.1365-2958.1998.01057.x.
7. Heath A, DiRita VJ, Barg NL, Engleberg NC. 1999. A two-component regulatory system, CsrR-CsrS, represses expression of three Streptococcus pyogenes virulence factors, hyaluronic acid capsule, streptolysin S, and pyrogenic exotoxin B. Infect Immun 67:5298–5305.
8. Federle MJ, McIver KS, Scott JR. 1999. A response regulator that represses transcription of several virulence operons in the group A *Streptococcus*. J Bacteriol 181:3649–3657.
9. Engleberg NC, Heath A, Miller A, Rivera C, DiRita VJ. 2001. Spontaneous mutations in the CsrRS two-component regulatory system of *Streptococcus pyogenes* result in enhanced virulence in a murine model of skin and soft tissue infection. J Infect Dis 183:1043–1054. https://doi.org/10.1086/319291.
10. Sumby P, Whitney AR, Graviss EA, DeLeo FR, Musser JM. 2006. Genome-wide analysis of group A streptococci reveals a mutation that modulates global phenotype and disease specificity. PLoS Pathog 2(1):e5. https://doi.org/10.1371/journal.ppat.0020005.
11. Kansal RG, Datta V, Aziz RK, Abdeltawab NF, Rowe S, Kotb M. 2010. Dissection of the molecular basis for hypervirulence of an in vivo-selected phenotype of the widely disseminated M1T1 strain of group A *Streptococcus* bacteria. J Infect Dis 201:855–865. https://doi.org/10.1086/651019.
12. Li J, Zhu H, Feng W, Liu M, Song Y, Zhang X, Zhou Y, Bei W, Lei B. 2013. Regulation of inhibition of neutrophil infiltration by the two-component regulatory system CovRS in subcutaneous murine infection with group A *Streptococcus*. Infect Immun 81:974–983. https://doi.org/10.1128/IAI.01218-12.
13. Li J, Liu G, Feng W, Zhou Y, Liu M, Wiley JA, Lei B. 2014. Neutrophils select hypervirulent CovRS mutants of M1T1 group A *Streptococcus* during subcutaneous infection of mice. Infect Immun 82:1579–1590. https://doi.org/10.1128/IAI.01458-13.
14. Stetzner ZW, Li D, Feng W, Liu M, Liu G, Wiley J, Lei B. 2015. Serotype M3 and M28 group A streptococci have distinct capacities to evade neutrophil and TNF-α responses and to invade soft tissues. PLoS One 10: e0129417. https://doi.org/10.1371/journal.pone.0129417.
15. Feng W, Minor D, Liu M, Li J, Ishaq SL, Yeoman C, Lei B. 2017. Null mutations of group A Streptococcus orphan kinase RocA: selection in mouse infection and comparison with CovS mutations in alteration of in vitro and in vivo protease SpeB expression and virulence. Infect Immun 85:e00790-16. https://doi.org/10.1128/IAI.00790-16.
16. Feng W, Minor D, Liu M, Lei B. 2017. Requirement and synergistic contribution of platelet-activating factor acetylhydrolase Sse and streptolysin S to inhibition of neutrophil recruitment and systemic infection by hypervirulent *emm*3 group A *Streptococcus* in subcutaneous infection of mice. Infect Immun 85:e00530-17. https://doi.org/10.1128/IAI.00530-17.
17. Daley JM, Thomay AA, Connolly MD, Reichner JS, Albina JE. 2008. Use of Ly6G-specific monoclonal antibody to deplete neutrophils in mice. J Leukoc Biol 83:64–70. https://doi.org/10.1189/jlb.0407247.
18. Bessen D, Fischetti VA. 1990. Synthetic peptide vaccine against mucosal colonization by group A streptococci. I. Protection against a heterologous M serotype with shared C repeat region epitopes. J Immunol 145:1251–1256.
19. Wessels MR, Moses AE, Goldberg JB, DiCesare TJ. 1991. Hyaluronic acid capsule is a virulence factor for mucoid group A streptococci. Proc Natl Acad Sci U S A 88:8317–8321.
20. Raeder R, Boyle MDP. 1993. Association between expression of immunoglobulin G-binding proteins by group A streptococci and virulence in a mouse skin infection model. Infect Immun 61:1378–1384.
21. Husmann LK, Dillehay DL, Jennings VM, Scott JR. 1996. Streptococcus pyogenes infection in mice. Microb Pathog 20:213–224. https://doi.org/10.1006/mpat.1996.0020.
22. Liu M, Zhu H, Zhang J, Lei B. 2007. Active and passive immunizations with the streptococcal esterase Sse protect mice against subcutaneous infection with group A streptococci. Infect Immun 75:3651–3657. https://doi.org/10.1128/IAI.00038-07.
23. Olsen RJ, Sitkiewicz I, Ayeras AA, Gonulal VE, Cantu C, Beres SB, Green NM, Lei B, Humbird T, Greaver J, Chang E, Ragasa WP, Montgomery CA, Cartwright J, Jr, McGeer A, Low DE, Whitney AR, Cagle PT, Blasdel TL, DeLeo FR, Musser JM. 2010. Decreased necrotizing fasciitis capacity caused by a single nucleotide mutation that alters a multiple gene virulence axis. Proc Natl Acad Sci U S A 107:888–893. https://doi.org/10.1073/pnas.0911811107.
24. National Research Council. 2011. Guide for the care and use of laboratory animals, 8th ed. National Academies Press, Washington, DC.
25. Beres SB, Sylva GL, Barbian KD, Lei B, Hoff JS, Mammarella ND, Liu MY, Smoot JC, Porcella SF, Parkins LD, Campbell DS, Smith TM, McCormick JK, Leung DY, Schlievert PM, Musser JM. 2002. Genome sequence of a serotype M3 strain of group A Streptococcus: phage-encoded toxins, the high-virulence phenotype, and clone emergence. Proc Natl Acad Sci U S A 99:10078–10083. https://doi.org/10.1073/pnas.152298499.
26. Zhu H, Liu M, Sumby P, Lei B. 2009. The secreted esterase of group A *Streptococcus* is important for invasive skin infection and dissemination in mice. Infect Immun 77:5225–5232. https://doi.org/10.1128/IAI.00636-09.